SUPPORTING INFORMATION

Pyrimidine-based Bipolar Host Materials for High Efficiency Solution Processed Green Thermally Activated Delayed Fluorescent OLEDs

Jiwon Yoon, Chiho Lee, Su Hong Park, Dong Won Kang, Hyojin Kim, Ji-Eun Jeong, Han Young Woo, Chang Seop Hong, Sungnam Park, Min Ju Cho* and Dong Hoon Choi*

Department of Chemistry, Research Institute for Natural Sciences, Korea University, 145, Anam-ro, Sungbuk-gu, Seoul 02841, Korea

*Corresponding authors: chominju@korea.ac.kr, dhchoi8803@korea.ac.kr

Table of Contents

3

1. Characterization

The molecular structures were determined by ^{1}H NMR and ^{13}C NMR spectra using Bruker 500 MHz and 125 MHz with $CDCl_3$ NMR solvent, respectively. Mass analyses were recorded to demonstrate the mass of the compounds by matrix-assisted laser desorption ionization time-of-flight mass spectrometry (MALDI-TOF/TOF™ 5800 system (AB SCIEX)) at the Korea Basic Science Institute (Seoul). Thermogravimetric analysis (TGA) and differential scanning calorimetry (DSC) measurements were performed at a heating ramp of 10 °C/min in N_2 by Mettler STAR^e. The optical and photophysical properties were determined by an Agilent 8453 (photodiode array = 190−1100 nm) spectrometer to obtain the UV−vis absorption spectra and HITACHI F-7000 spectrometer to obtain the room temperature and low-temperature PL spectra. The absolute PL quantum yield (PLQY) of doped films was obtained using a JASCO FP-8600 with a Xenon lamp excitation source, using 90° angle detection for solution samples, and was obtained by detecting all sample fluorescence using an integrating sphere (ILF-835, JASCO) and comparing with incident light. The transient photoluminescence (TRPL) measurements at room temperature were evaluated under a nitrogen atmosphere. A train of 1064 nm pulses with durations of 5 ns was produced at 10 Hz from a Nd:YAG laser (Powerlite Precision II 8000, Continuum). A 355-nm pulse was obtained by the generation of the third harmonic and was used to directly excite the film sample cast on an optical glass. The emission from the film sample was collected using a lens (focal length = 10 cm), passed through a monochromator, and detected using a photomultiplier tube (PMT) connected to a 100 MHz digital oscilloscope (DSO-X 3014A, Keysight). Cyclic voltammetry (CV) was performed using a EA161, eDAQ for the neat film of the host material to obtain the oxidation properties. A 0.10 M solution of

tetrabutylammonium hexafluorophosphate (Bu$_4$NPF$_6$) in acetonitrile was used as the supporting electrolyte for neat films. Ag/AgCl and Pt wire (diameter 0.5 mm) were used as reference and counter electrodes, respectively. Atomic force microscopy (AFM, XE-100 advanced scanning probe microscope, PSIA) in the tapping mode was performed to investigate the surface morphologies of the spin-coated films.

2. Theoretical Calculations

The optimized molecular structures, frontier molecular orbitals (HOMO and LUMO), and excited states (S$_1$ and T$_1$ state) of **Py2Cz**, **Py2BFCz**, and **Py2ICz** were calculated using the density functional theory (DFT) with the B3LYP functional and 6-31G(d) basis set implemented in the commercial Gaussian 16 software package.[1]

3. Device Fabrication and Measurements

The green TADF device structure was indium tin oxide (ITO)/poly(3,4-ethylenedioxythiophene):poly(styrenesulfonic acid) (PEDOT:PSS, 40 nm)/poly-(9-vinylcarbazole) (PVK, 20 nm)/**Py2Cz** or **Py2BFCz** or **Py2ICz** : **t4CzIPN** (15 nm, 3, 6, and 9 wt%)/1,3,5-tris(1-phenyl-1*H*-benzimidazol-2-yl)benzene (TPBi, 40 nm)/LiF (0.8 nm)/Al (100 nm). An ITO-coated glass, which has a sheet resistance of 10 Ω/sq, was used as the anode, and an active pattern was formed with an area of 2 × 2 mm^2. Before device fabrication, the ITO-coated substrates were sequentially washed in an ultrasonic bath with deionized water and 2 times of isopropyl alcohol for 10 min each. The cleaned ITO-coated substrates were dried in a vacuum oven. The dried ITO-coated substrates were treated in a UV-ozone

chamber for 20 min. PEDOT:PSS (40 nm) was spin-coated on the ITO-coated substrates at 4000 rpm for 30 s and then annealed at 155 °C for 15 min. The 0.5 wt% PVK solution was prepared from a chlorobenzene solvent, and spin-coated on top of the ITO/PEDOT:PSS, and then annealed at 130 °C for 20 min. The emitting layers were prepared from a toluene solution and spin-coated at 3000 rpm for 30 s. A TPBi with a thickness of 40 nm was deposited under a high vacuum. Lastly, LiF and Al were deposited sequentially under a high vacuum environment. The OLED devices, which have current density−voltage−luminance ($J{-}V{-}L$) characteristics, were measured with a Keithley SMU 236 instrument and SpectraScan PR-655 colorimeter. Furthermore, the fabricated structure of the hole-only devices (HODs) was ITO/PEDOT:PSS (40 nm)/ PVK (20 nm)/**Py2Cz** or **Py2BFCz** or **Py2ICz** (15 nm)/Al (100 nm) and that of the electron-only devices (EODs) was ITO/ **Py2Cz** or **Py2BFCz** or **Py2ICz** (15 nm)/ TPBi (40 nm)/ LiF (0.8 nm)/ Al (100 nm). The current density–voltage (J–V) data were measured using a Keithley SMU 236 instrument.

4. X-ray Diffraction and Refinement

Single crystal analysis data for **Py2Cz** was collected using a Bruker SMART APEXII diffractometer equipped with a graphite monochromated MoKα radiation source ($\lambda = 0.71073$ Å). The preliminary orientation matrix and cell parameters were determined from three sets of ω scans at different starting angles. Data frames were obtained at scan intervals of 0.5° with an exposure time of 30 s per frame. The reflection data were corrected for Lorentz and polarization factors. Absorption corrections were carried out using SADABS.[2] The structures were solved by direct methods and refined by full-matrix least-squares analysis using

anisotropic thermal parameters for non-hydrogen atoms with the SHELXTL program.[3] All hydrogen atoms were calculated at idealized positions and refined with the riding models.

Single crystal analysis data for **Py2BFCz** was mounted on a cryoloop under a cooling stream of dinitrogen. Diffraction data were collected with synchrotron radiation using a 2D-SMC ADSC Quantum-210 detector with a Pt-coated Si double crystal under a cooling stream of N_2 at the Pohang Accelerator Laboratory. The ADSC Quantum-210 ADX program was used for data collection, and HKL3000 was used for cell refinement, data reduction, and absorption corrections. The structure was solved by direct methods and refined by full-matrix least-squares analysis using anisotropic thermal parameters for non-hydrogen atoms with the SHELXTL program.[4] Guest molecules in the lattice were highly disordered and could not be modeled. To account for this electron density, the program SQUEEZE, a part of the PLATON package of crystallographic software, was used to calculate the solvent disorder area and remove its effect to the overall intensity data.[5, 6] All hydrogen atoms except for hydrogen bound to water oxygen atoms were calculated at idealized positions and refined with the riding models. Drawings were produced using Mercury 4.1.2. CCDC-1956945 (**Py2Cz**) and CCDC-1956946 (**Py2BFCz**) contain supplementary crystallographic data. These data can be obtained free of charge from the Cambridge Crystallographic Data Centre *via* www.ccdc.cam.ac.uk/data_request/cif.

5. Experimental Determination of the Activation Energy (E_a) for Reverse Intersystem Crossing

To measure the activation energy (E_a) for the RISC of **t4CzIPN** in various host films, TRPL

signals were measured at different temperatures. k_{RISC} was obtained from the kinetic analysis of the TRPL signal at each temperature. $\ln(k_{RISC})$ was plotted against $1/T$ (i.e., the Arrhenius plot), and the activation energy (E_a) was determined from the slope ($= -E_a/R$) of the Arrhenius plot.

**Table S1**. Summary of crystal data and structure refinement for **Py2Cz** and **Py2BFCz**.

| Identification code	Py2Cz	Py2BFCz
Empirical formula	$C_{46}H_{30}N_4$	$C_{58}H_{34}N_4O_2$
Formula weight	638.74	818.89
Temperature	296(2) K	100(2) K
Wavelength	0.711 Å	0.700 Å
Crystal system	Monoclinic	Triclinic
Space group	P 21 / c	P-1
Unit cell dimensions	a = 9.427(3) Å b = 19.529(5) Å c = 18.192(5) Å α = 90.00 º β = 91.10(19)º γ = 90.00 º	a = 11.992(2) Å b = 13.363(3) Å c = 14.792(3) Å α = 66.13(3)º β = 86.11(3)º γ = 74.84(3)º
Volume	3348.3(16) Å^3	2090.3(9) Å^3
Z	4	2
Density (calculated)	1.267 g/cm^{-3}	1.301 g/cm^{-3}
Absorption coefficient	0.075 mm^{-1}	0.086 mm^{-1}
F(000)	1336	852
Crystal size	0.400 × 0.300 × 0.200 mm^3	0.100 × 0.050 × 0.030 mm^3
Theta range for data collection	2.399 to 28.296°	1.484 to 32.753°
Index ranges	-12 ≤ h ≤ 12, -26 ≤ k ≤ 25, - 22≤ l ≤ 24	-18 ≤ h ≤ 17, -16 ≤ k ≤ 17, -20 ≤ l ≤ 21
Reflections collected	60224	16654
Independent reflections	8302 [R(int) = 0.1195]	9314 [R(int) = 0.0417]
Completeness to theta	25.242 º, 99.9 %	24.835 º, 90.7 %
Absorption correction	-	Empirical
Max. and min. transmission	0.7457 and 0.7129	1.000 and 0.753
Refinement method	Full-matrix least-squares on F^2	Full-matrix least-squares on F^2
Data/restraints/parameters	8302 / 0 / 452	9314 / 0 /577
Goodness-of-fit on F^2	0.945	1.013
Final R indices [I>2sigma(I)]	R_1 = 0.0604, wR_2 = 0.1319	R_1 = 0.0588, wR_2 = 0.1578
R indices (all data)	R_1 = 0.2113, wR_2 = 0.1894	R_1 = 0.0902, wR_2 = 0.1733
Extinction coefficient	0.0082(9)	n/a
Largest diff. peak and hole	0.189 and -0.157 e. Å^{-3}	0.312 and -0.275 e. Å^{-3}
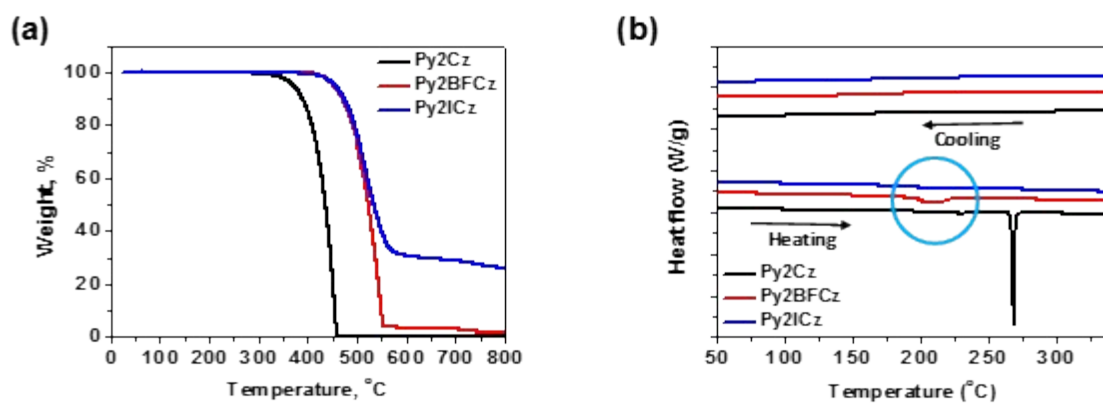
Fig. S1 (a) TGA and (b) DSC traces of **Py2Cz**, **Py2BFCz**, and **Py2ICz** recorded at a heating rate of 10 °C/min under a nitrogen atmosphere.
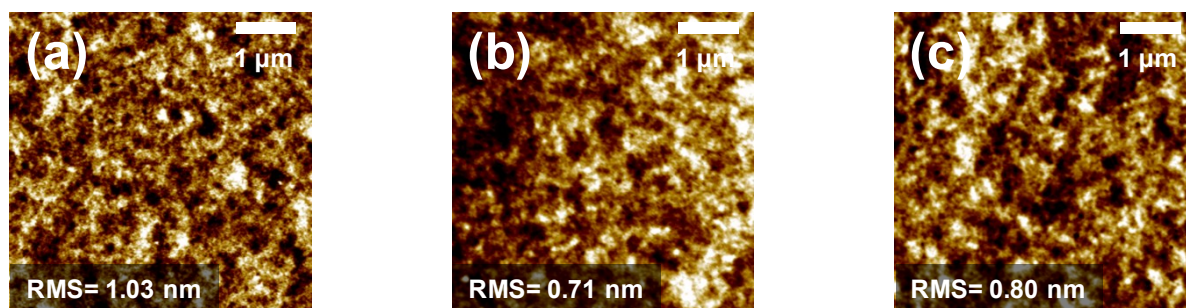
Fig. S2. AFM topographic images of solution-processed films (5.0 μm × 5.0 μm) of **t4CzIPN** doped (a) **Py2Cz**, (b) **Py2BFCz**, and (c) **Py2ICz**.
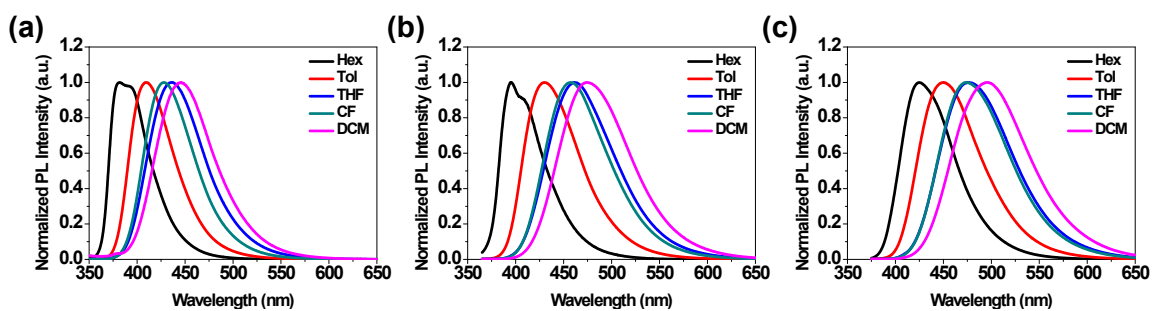
Fig. S3. PL spectra of (a) **Py2Cz**, (b) **Py2BFCz**, and (c) **Py2ICz** in different solvents. Concentration: 1.0×10^{-5} M
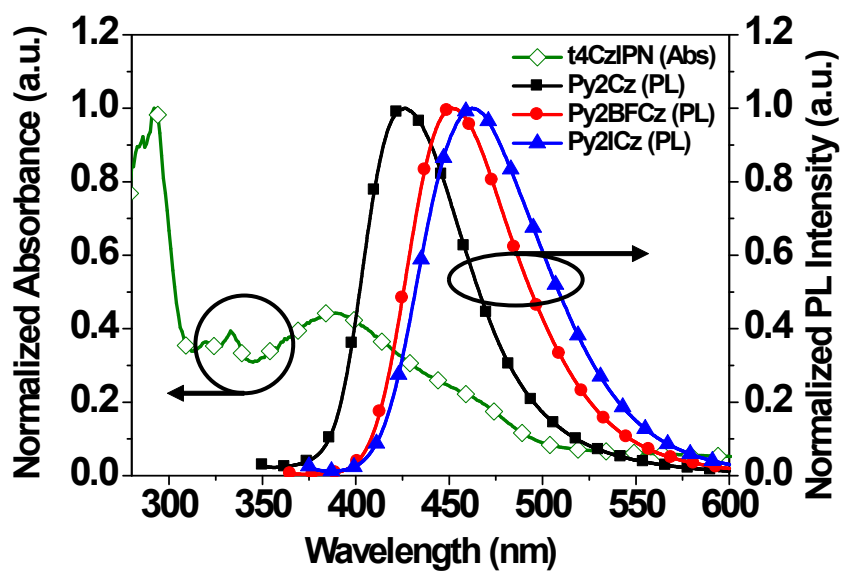
Fig. S4. UV–vis absorption spectrum of **t4CzIPN** compared with PL spectra of **Py2Cz**, **Py2BFCz**, and **Py2ICz** in neat films.
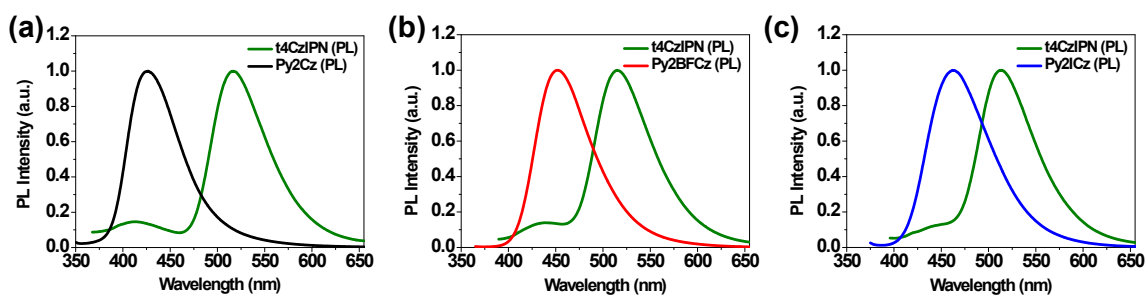
Fig. S5. PL spectra of **t4CzIPN** doped (a) **Py2Cz**, (b) **Py2BFCz**, and (c) **Py2ICz** films and those of only **Py2Cz**, **Py2BFCz**, and **Py2ICz**, respectively.
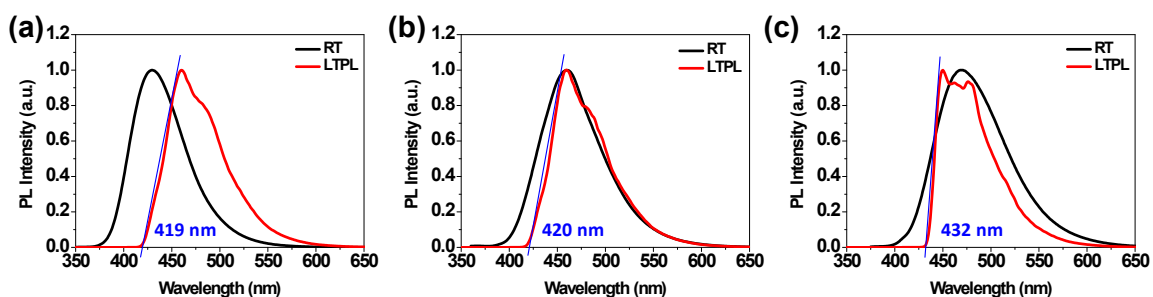
Fig. S6. Room-temperature (RT) and low-temperature PL (LTPL) spectra of (a) **Py2Cz**, (b) **Py2BFCz**, and (c) **Py2ICz** in 2-methyltetrahydrofuran solution.
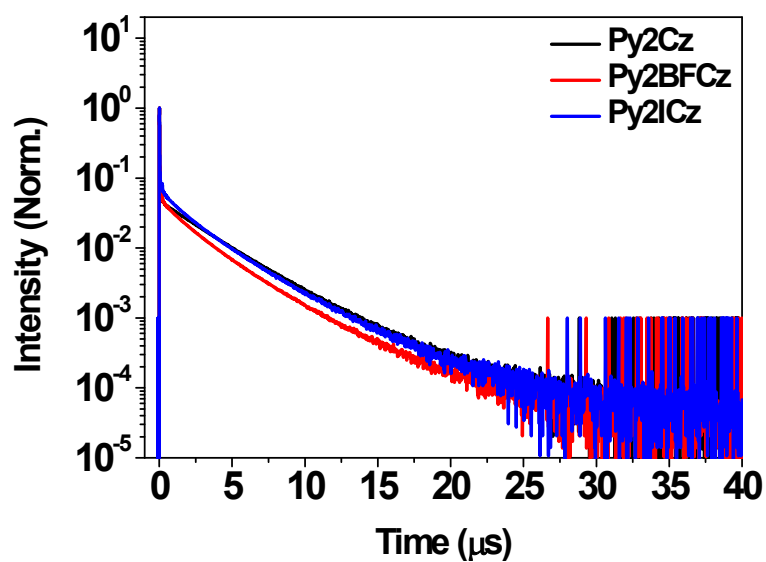
Fig. S7. Transient PL spectra of 6 wt% **t4CzIPN** doped **Py2Cz**, **Py2BFCz**, and **Py2ICz** films at room temperature.

Table S2. Photophysical properties and kinetic parameters of 6 wt% **t4CzIPN** doped **Py2Cz**, **Py2BFCz**, and **Py2ICz** films at room temperature.

Host	τ_p (ns)	τ_d (µs)	Φ_{PL} (%)	Φ_p (%)	Φ_d (%)
Py2Cz	16.09	3.385	68.5	6.3	62.2
Py2BFCz	18.38	2.724	57.2	7.3	49.9
Py2ICz	24.07	2.863	61.7	7.4	54.3
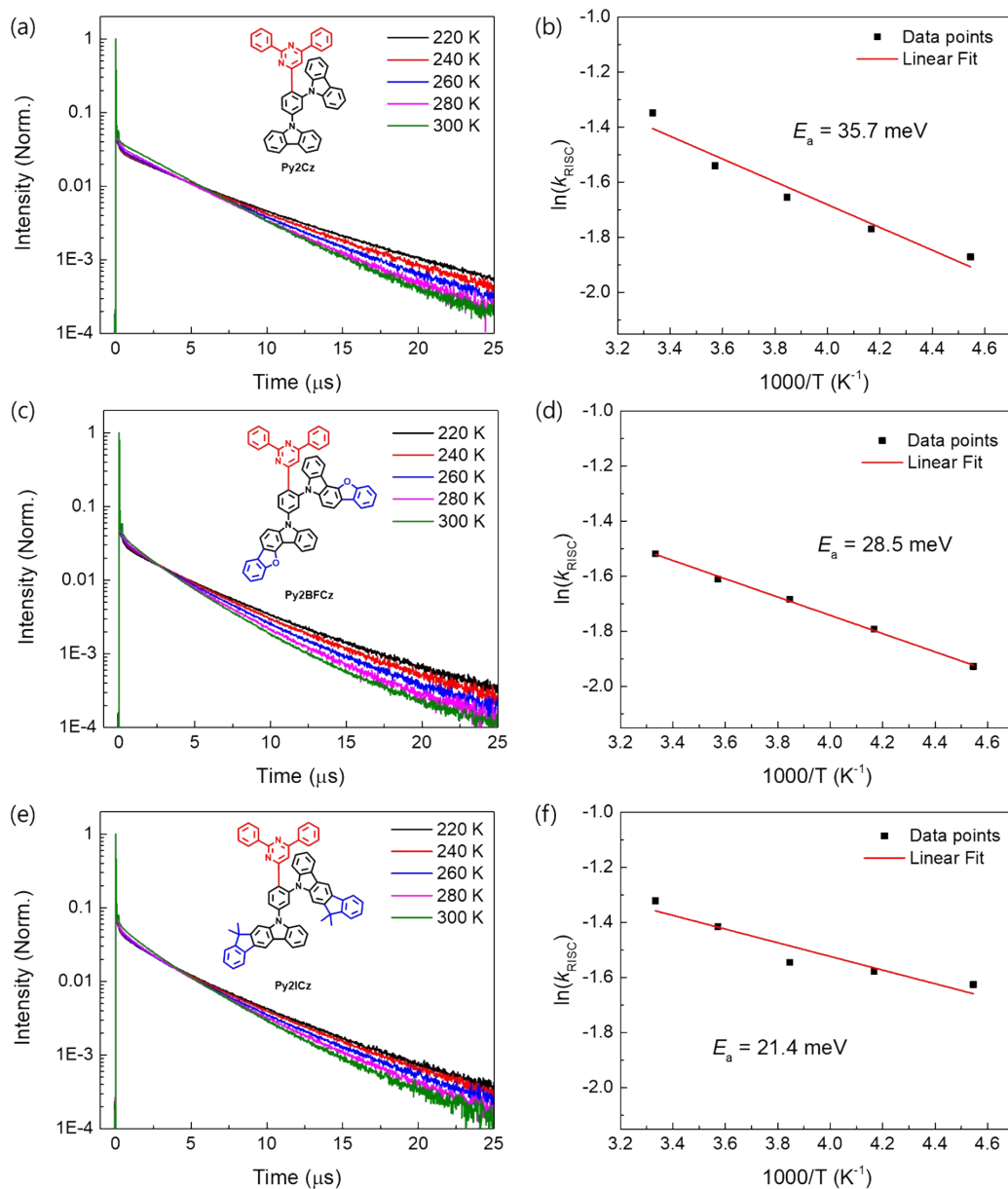
Fig. S8. (a), (c), and (e) TRPL signals of **t4CzIPN** in the films of **Py2Cz**, **Py2BFCz**, and **Py2ICz**. The temperature of the film samples was increased gradually from 220 K to 300 K at intervals of 20 K. (b), (d), and (f) show Arrhenius plots and E_a.
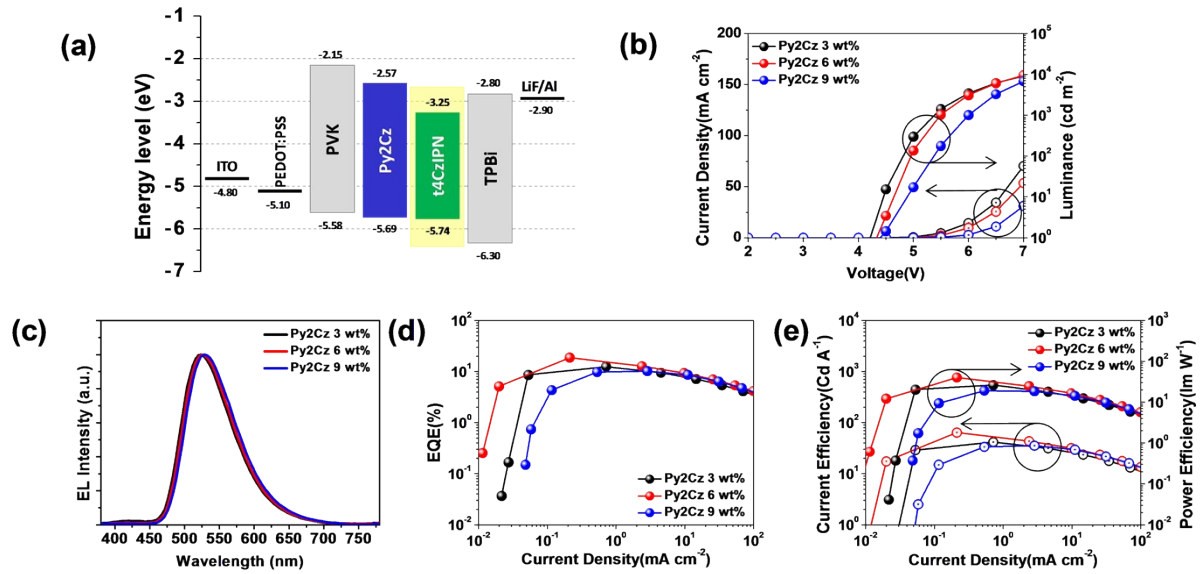
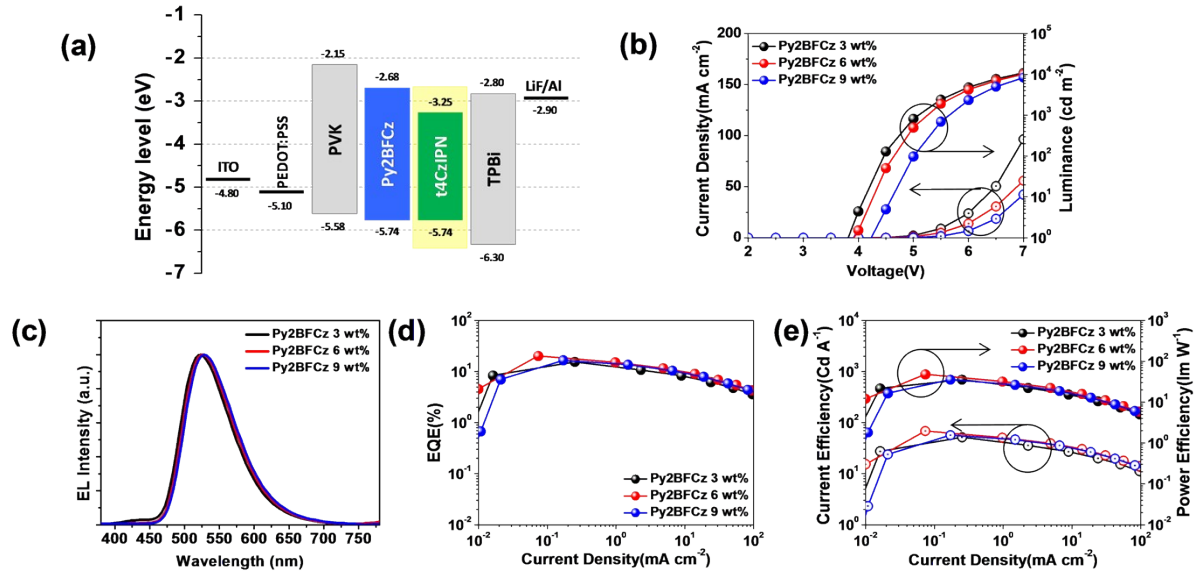**Fig. S9.** (a) Device configurations, (b) *J–V–L* characteristics, (c) EL spectra of green TADF OLEDs at 1000 cd/m², (d) EQE–*J* curves, and (e) CE–*J*–PE curves.

Table S3. Device performances of green TADF OLEDs with **t4CzIPN**.

Host	Doping concentration	V_{on} [a] (V)	CE_{max} [b] (cd·A⁻¹)	PE_{max} [c] (lm·W⁻¹)	EQE_{max} [d] (%)	At 500 cd·m⁻² EQE (%)	At 1000 cd·m⁻² EQE (%)	CIE (x,y) [e]
Py2Cz	3 wt%	4.1	41.7	26.2	12.5	11.9	10.5	(0.31,0.58)
	6 wt%	4.3	64.1	40.3	18.8	16.1	13.0	(0.32,0.59)
	9 wt%	4.5	35.3	19.2	10.3	10.0	10.3	(0.33,0.59)

[a] Turn-on voltage at 1 cd/m²; [b] CE_{max} = maximum current efficiency [c] PE_{max} = maximum power efficiency; [d] EQE_{max} = external quantum efficiency; [e] at 1000 cd·m⁻².

Fig. S10. (a) Device configurations, (b) *J-V-L* characteristics, (c) EL spectra of green TADF OLEDs at 1000 cd/m², (d) EQE-*J* curves, and (e) CE-*J*-PE curves.

Table S4. Device performances of green TADF OLEDs with **t4CzIPN**.

Host	Doping concentration	V_{on} [a] (V)	CE_{max} [b] (cd·A⁻¹)	PE_{max} [c] (lm·W⁻¹)	EQE_{max} [d] (%)	At 500 cd·m⁻² EQE (%)	At 1000 cd·m⁻² EQE (%)	CIE (x,y) [e]
Py2BFCz	3 wt%	3.7	51.4	35.9	15.5	12.8	10.5	(0.30,0.58)
	6 wt%	4.0	68.8	48.0	20.2	15.0	13.8	(0.32,0.59)
	9 wt%	4.1	57.0	35.8	16.6	14.5	13.0	(0.33,0.59)

[a] Turn-on voltage at 1 cd/m²; [b] CE_{max} = maximum current efficiency [c] PE_{max} = maximum power efficiency; [d] EQE_{max} = external quantum efficiency; [e] at 1000 cd·m⁻².
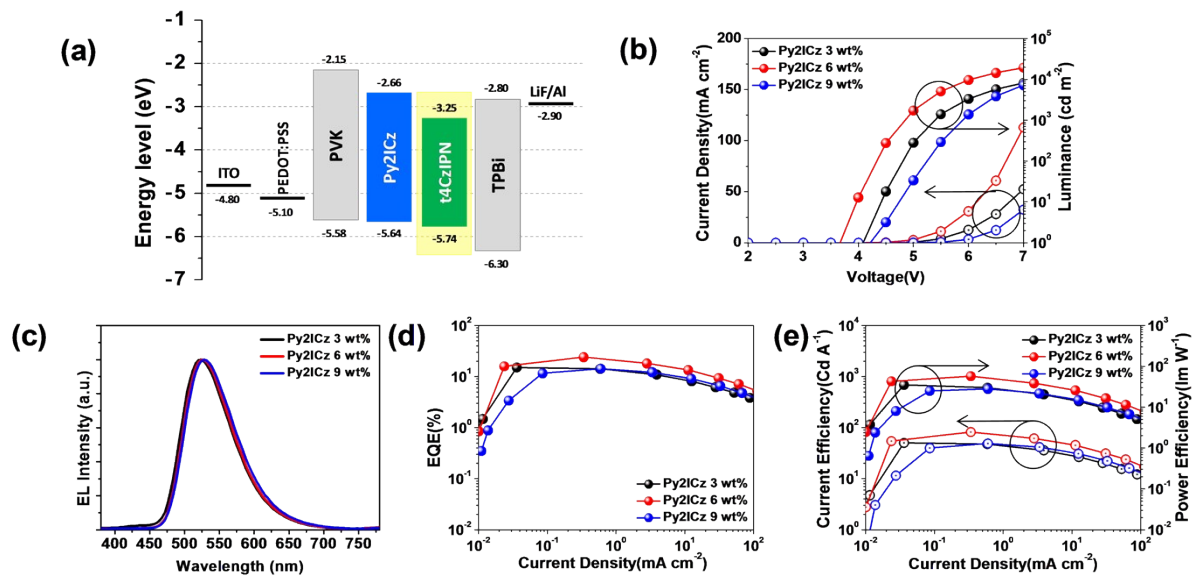
Fig. S11. (a) Device configurations, (b) *J–V–L* characteristics, (c) EL spectra of green TADF OLEDs at 1000 cd/m^2, (d) EQE–*J* curves, and (e) CE–*J*–PE curves.

Table S5. Device performances of green TADF OLEDs with **t4CzIPN**.

Host	Doping concentration	V_{on} [a] (V)	CE_{max} [b] (cd·A^{-1})	PE_{max} [c] (lm·W^{-1})	EQE_{max} [d] (%)	At 500 cd·m^{-2} EQE (%)	At 1000 cd·m^{-2} EQE (%)	CIE (x,y) [e]
Py2ICz	3 wt%	4.0	50.3	35.1	15.0	13.5	12.0	(0.31,0.58)
	6 wt%	3.6	82.1	57.3	24.1	23.0	21.0	(0.32,0.60)
	9 wt%	4.2	49.0	28.0	14.3	13.9	13.0	(0.33,0.59)

[a] Turn-on voltage at 1 cd/m^2; [b] CE_{max} = maximum current efficiency [c] PE_{max} = maximum power efficiency; [d] EQE_{max} = external quantum efficiency; [e] at 1000 cd·m^{-2}.

Table S6. Present solution-processed device performance using **t4CzIPN** dopant.

Host	Device structure	V^{a} (V)	CE_{max}^{b} (cd·A^{-1})	PE_{max}^{c} (lm·W^{-1})	EQE_{max}^{d} (%)	CIE (x,y) ^{e}	Ref.
Py2Cz	ITO/PEDOT:PSS (40 nm)/PVK (20 nm)/host:6 wt% t4CzIPN (15 nm)/TPBi (40 nm)/LiF (0.8 nm)/Al (100 nm)	4.3	64.1	40.3	18.8	(0.32, 0.59)	
Py2BFCz		4.0	68.8	48.0	20.2	(0.32, 0.59)	**In this work**
Py2ICz		3.6	82.1	57.3	24.1	(0.32, 0.60)	
IAPC	ITO (150 nm)/PEDOT:PSS (40 nm)/PVK (20 nm)/IAPC:6 wt% t4CzIPN (20 nm)/TPBi (40 nm)/LiF (0.8 nm)/Al (100 nm)	3.9	58.3	33.3	17.4	(0.31, 0.59)	7
SiCT	ITO(150 nm)/PEDOT:PSS (40 nm)/PVK (10 nm)/SiCT:t4CzIPN (20 nm)/TPBi (40 nm)/LiF (0.8 nm)/Al (100 nm)	4.5	65.5	41.1	19.2	(0.34, 0.59)	8
CDPO	ITO (150 nm)/PEDOT:PSS (40 nm)/PVK (10 nm)/host: t4CzIPN (20 nm, 2 wt%)/TPBi (40 nm)/LiF (0.8 nm)/Al (100 nm)	5.7	37.4	16.8	11.8	(0.28, 0.56)	9
mCPDPO		5.5	61.5	29.7	18.8	(0.31, 0.58)	
SiCz	ITO(120 nm)/PEDOT:PSS (60 nm)/PVK (15 nm)/SiCz:t4CzIPN (25 nm, 1 % doping)/TSPO1 (5 nm)/TPBi (30 nm)/LiF (1 nm)/Al (100 nm)	-	-	42.7	18.3	(0.31, 0.59)	10

[a] at 1 cd/m^{2}; [b] CE$_{max}$ = maximum current efficiency [c] PE$_{max}$ = maximum power efficiency; [d] EQE$_{max}$ = external quantum efficiency; [e] at 1000 cd·m^{-2}.
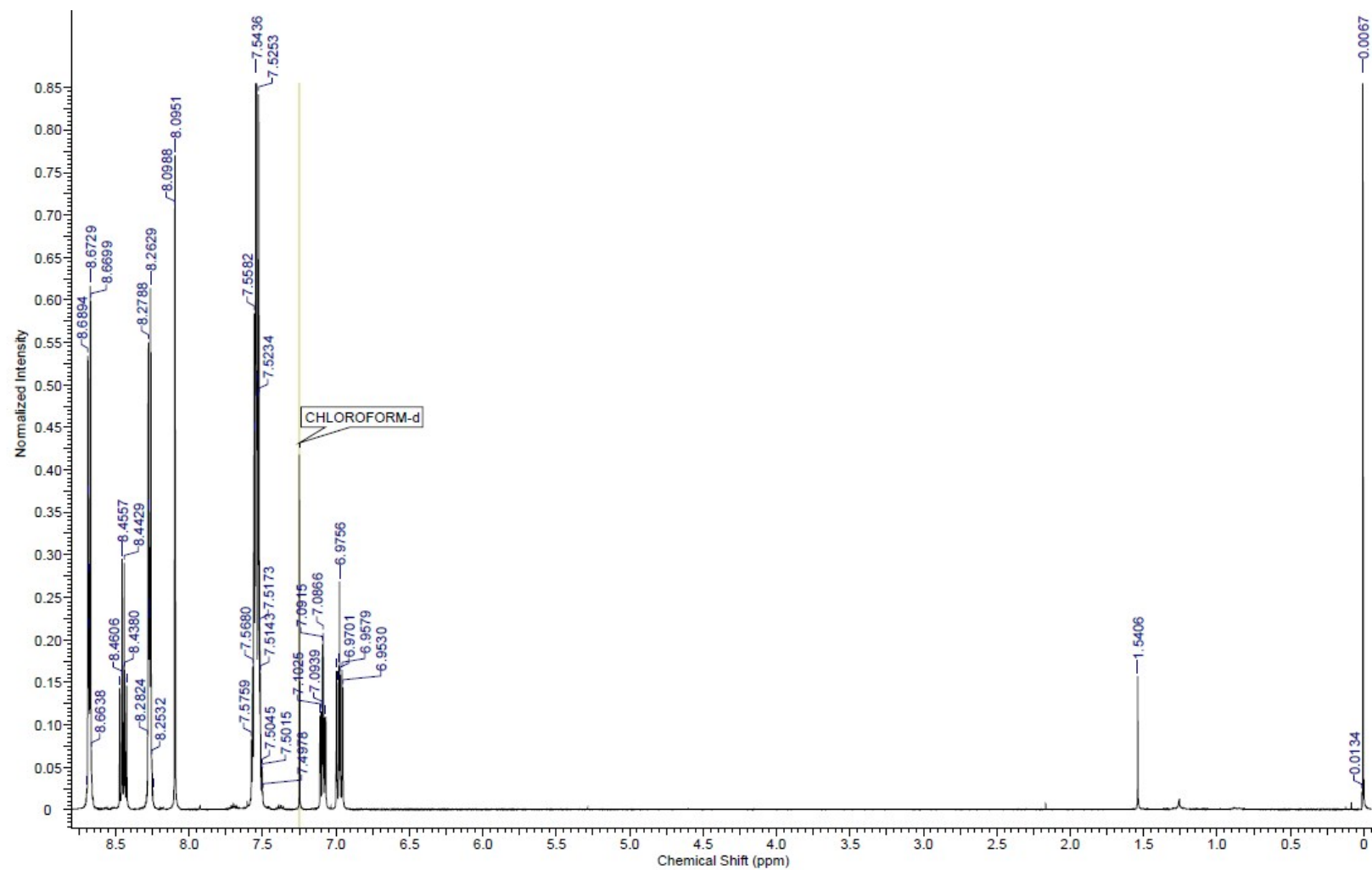
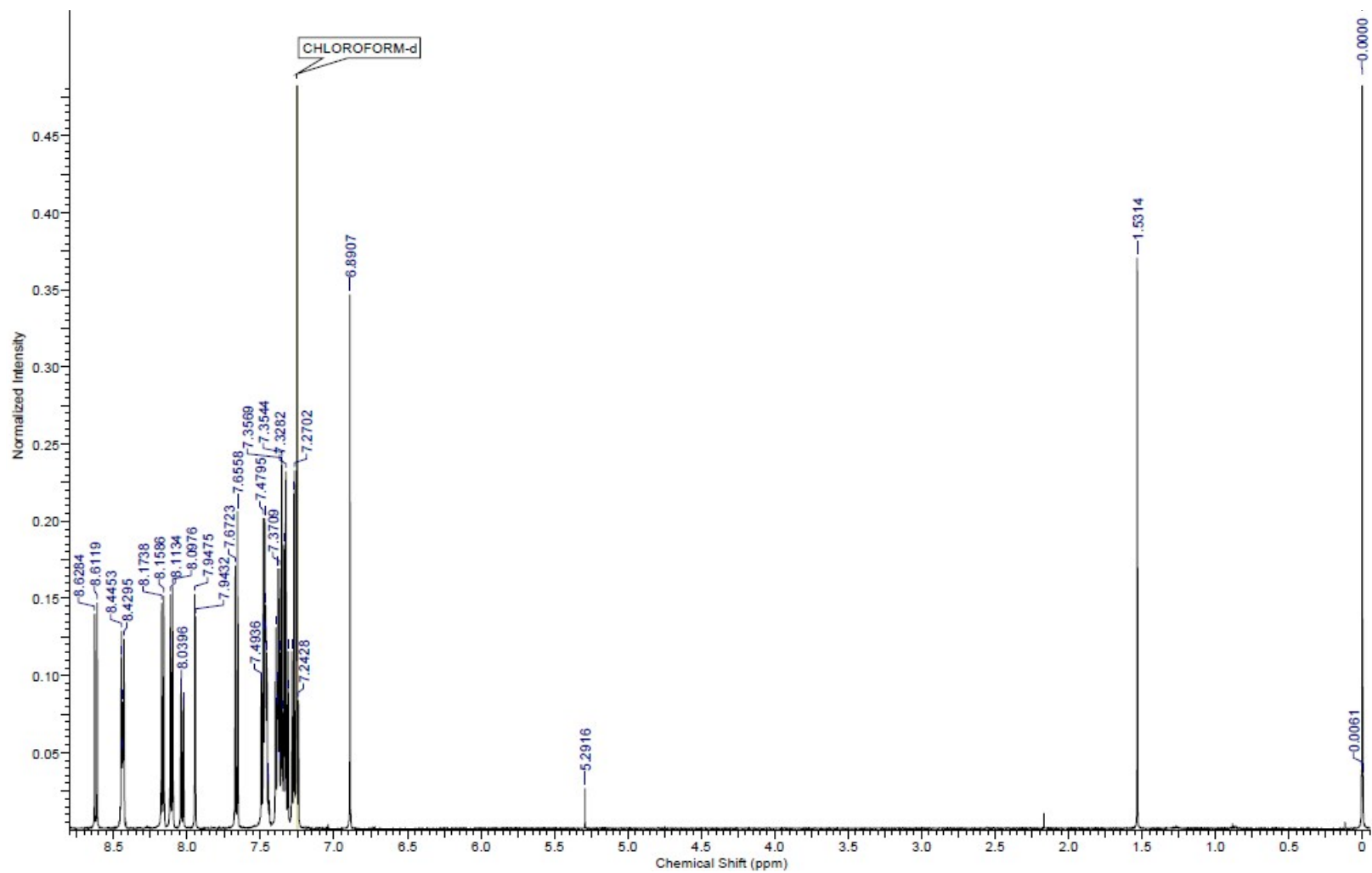**Fig. S12**. ^{1}H NMR spectrum of **4-(2,4-difluorophenyl)-2,6-diphenylpyrimidine**.

Fig. S13. ^{1}H NMR spectrum of **Py2Cz**.
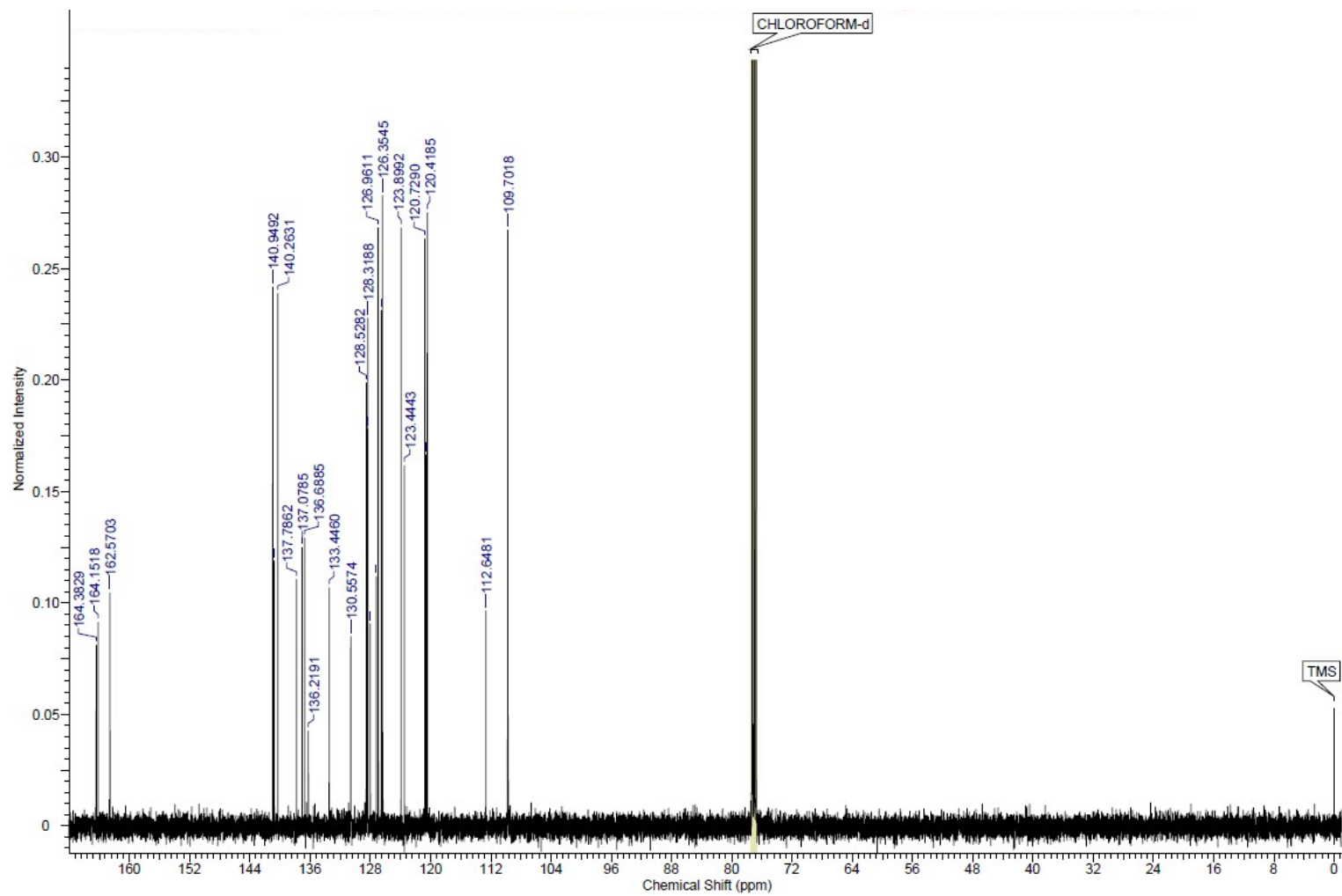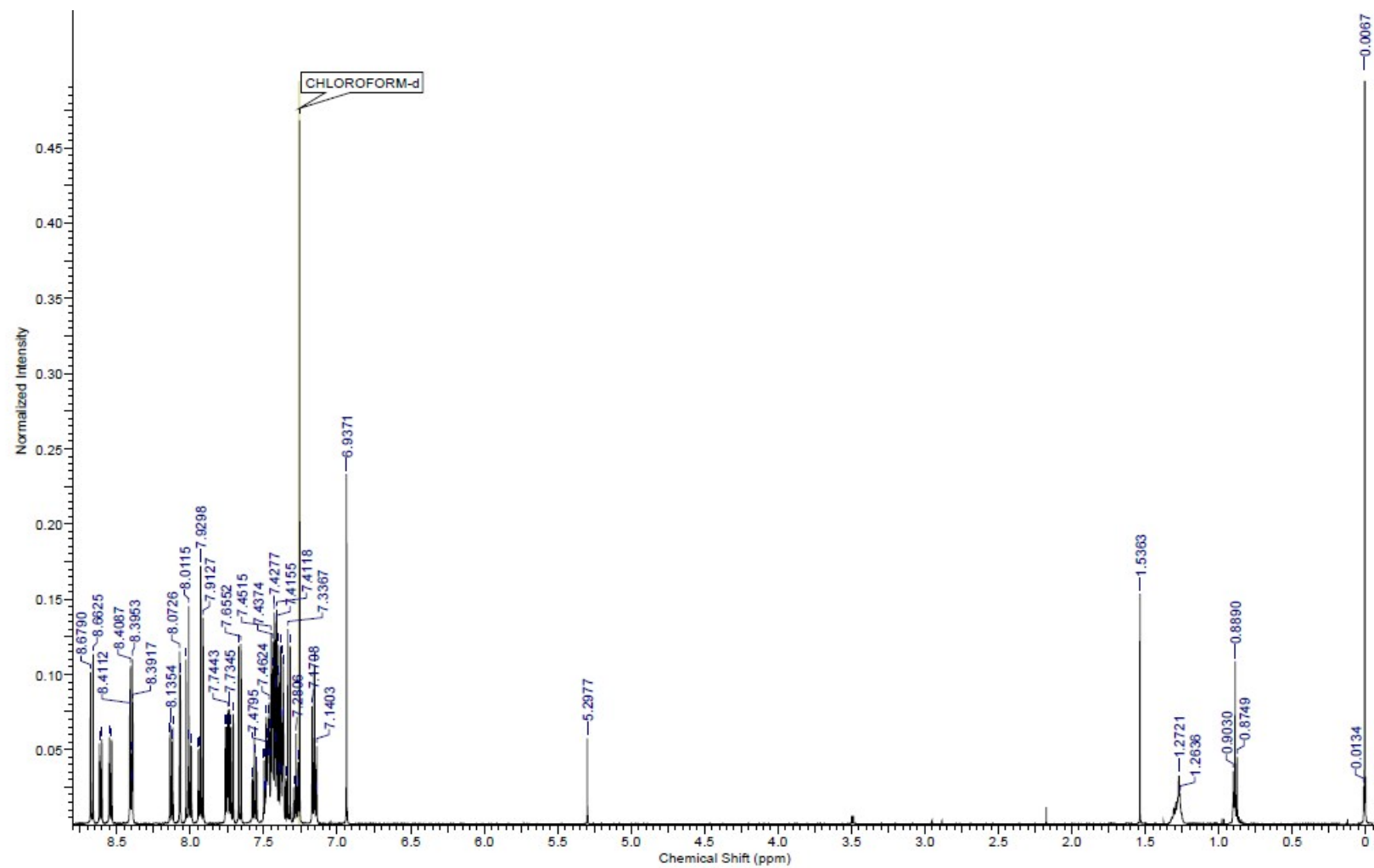
Fig. S14. ^{13}C NMR spectrum of **Py2Cz**.

Fig. S15. ^{1}H NMR spectrum of **Py2BFCz**.
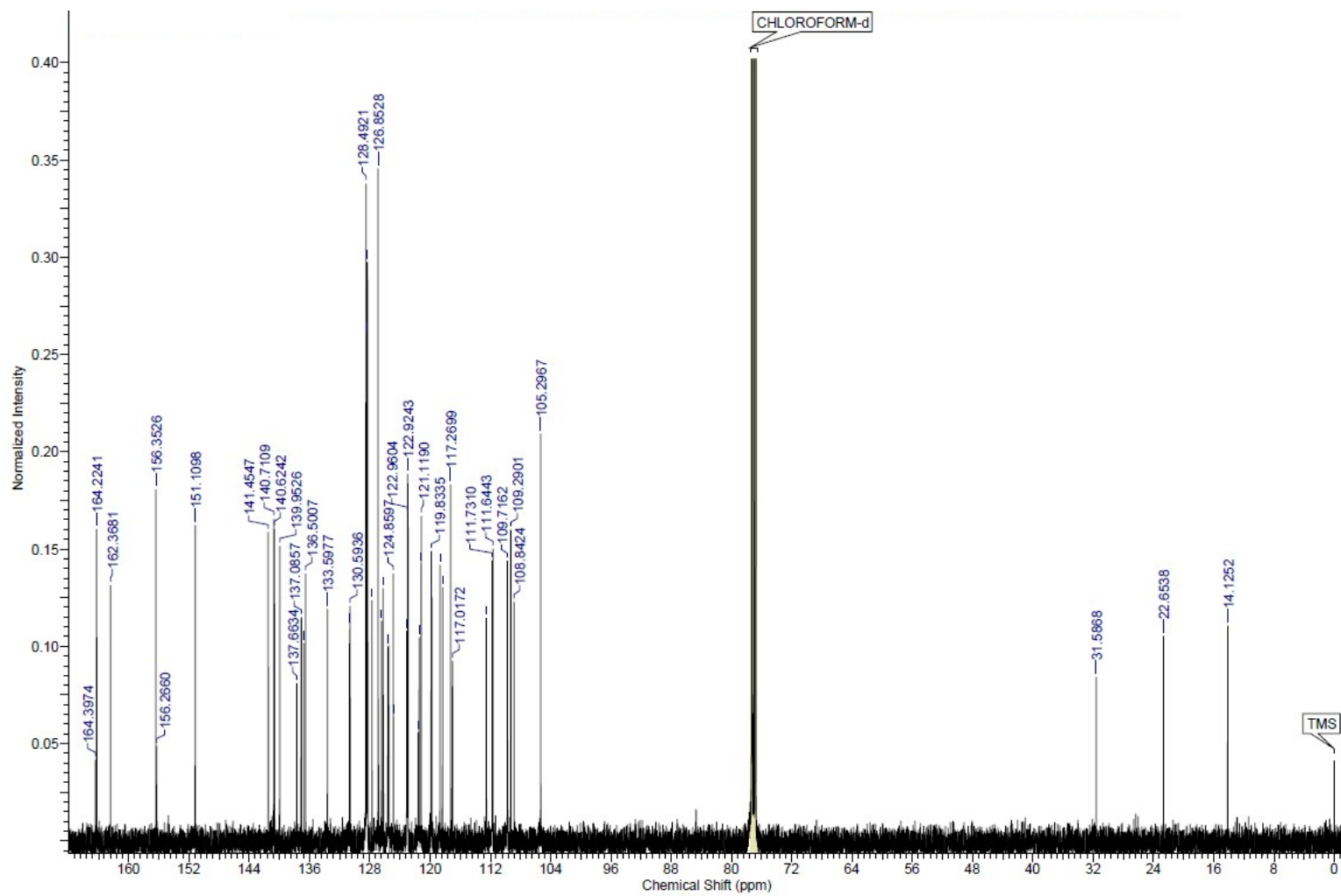
Fig. S16. ^{13}C NMR spectrum of **Py2BFCz**.
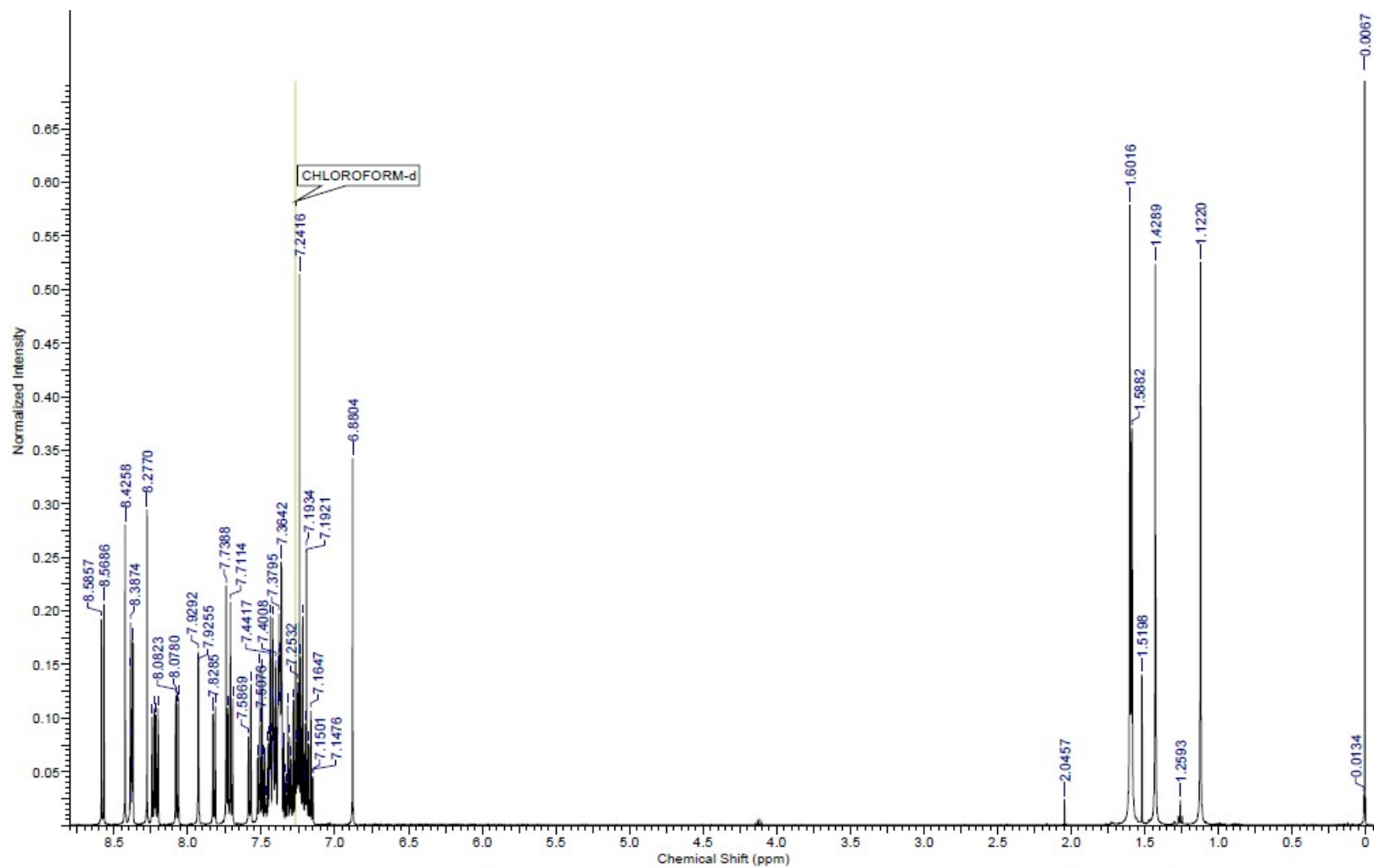
Fig. S17. ^{1}H NMR spectrum of **Py2ICz**.

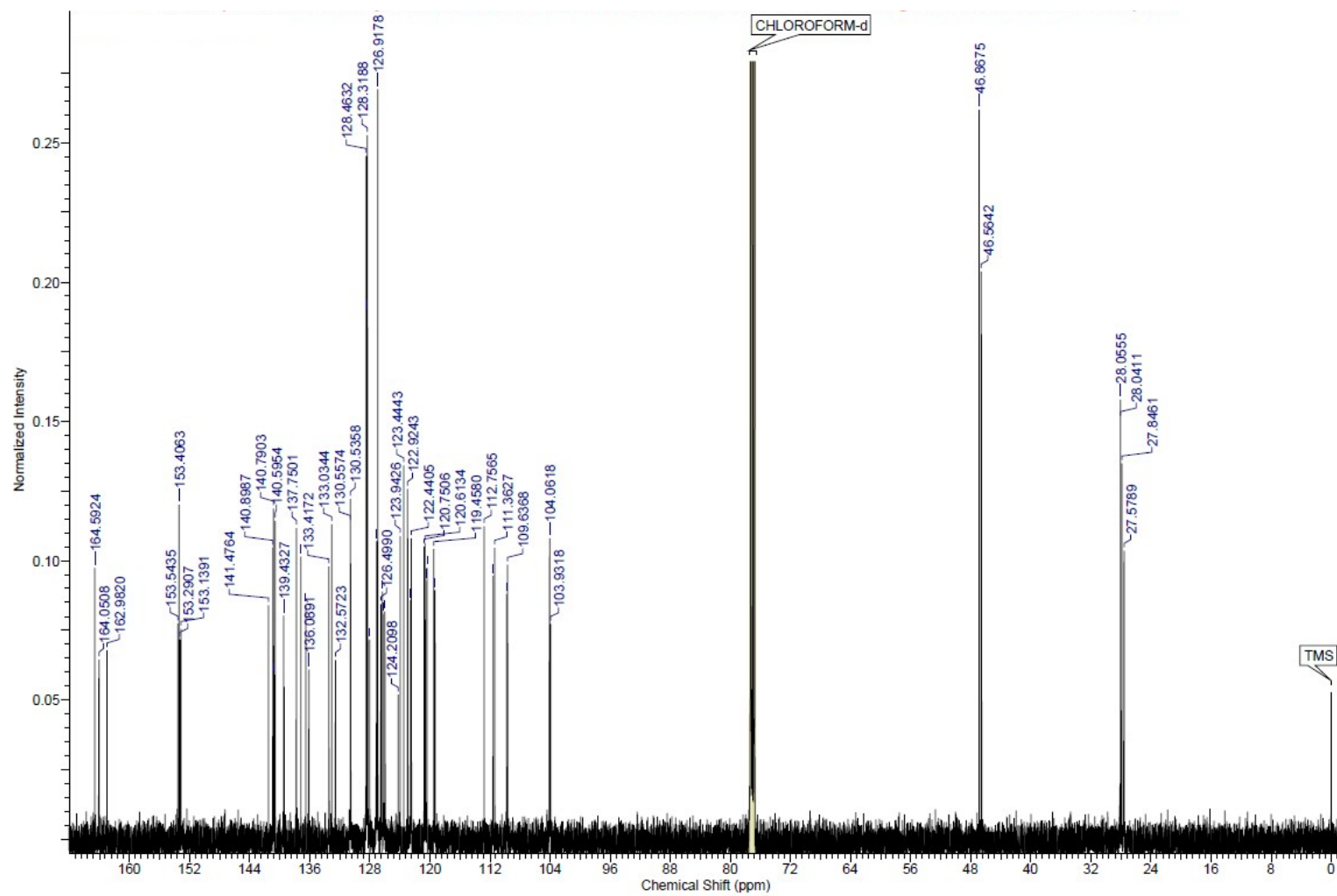**Fig.** **S18**. ^{13}C NMR spectrum of **Py2ICz**.

REFERENCES

[1]   M. J. Frisch, G. W. Trucks, H. B. Schlegel, G. E. Scuseria, M. A. Robb, J. R. Cheeseman, G. Scalmani, V. Barone, G. A. Petersson and H. Nakatsuji et al., *Gaussian 16 Rev. A.03*, Wallingford, CT, **2016**.

[2]   G. M. Sheldrick, SADABS, A program for area detector absorption corrections, University of Gottingen, Germany, **1994**.

[3]   G. M. Sheldrick, SHELXTL, Version 5, Bruker AXS, Madison, Wisconsin. **1995**.

[4]   G. M. Sheldrick, *SHELXTL,Version6.12, Bruker Analytical X-raySystems,Inc.,Madison,* **2000**.

[5]   A. L. Spek, *Acta Crystallogr., Sect. A Fundam. Crystallogr.*, 1990, **46**, 1.

[6]   Sluis, v. d. P.; Spek, A. L., BYPASS:, *Acta Crystallogr. Sect. A Fundam. Crystallogr.*, 1990, **A46**, 194-201.

[7]   C. H. Jeong, M. Godumala, J. Yoon, S. Choi, Y. W. Kim, D. H. Choi, M. J. Cho and D. H. Choi, *ACS Appl. Mater. Interfaces*, 2019, **11**, 17602-17609.

[8]   S. Choi, J. Yoon, M. Godumala, H. J. Kim, S. H. Park, S. K. Kim, H. Lee, J. H. Kwon, M. J. Cho and D. H. Choi, *Dyes and Pigments*, 2019, **167**, 120-126.

[9]   M. Godumala, S. Choi, S. K. Kim, S. W. Kim, J. H. Kwon, M. J. Cho and D. H. Choi, *J. Mater. Chem. C*, 2018, **6**, 10000-10009.

[10]   Y. J. Cho, K. S. Yook and J. Y. Lee, *Adv. Mater.*, 2014, **26**, 6642-6646.